We are IntechOpen, the world's leading publisher of Open Access books Built by scientists, for scientists

6,900
Open access books available

185,000
International authors and editors

200M
Downloads

Our authors are among the

154
Countries delivered to

TOP 1%
most cited scientists

12.2%
Contributors from top 500 universities



WEB OF SCIENCE™

Selection of our books indexed in the Book Citation Index in Web of Science™ Core Collection (BKCI)

Interested in publishing with us?
Contact book.department@intechopen.com

Numbers displayed above are based on latest data collected.
For more information visit www.intechopen.com



3

Ventilation Effectiveness Measurements Using Tracer Gas Technique

Hwataik Han
Kookmin University
Korea

1. Introduction

Ventilation effectiveness has been defined in various ways by many investigators. The term *ventilation efficiency* was first used by Yaglou and Witheridge (1937). They defined it as the ratio of the carbon dioxide concentration in a room to that in the extract duct. The ventilation was considered to be effective if the air contaminants in high concentration level are captured by the exhaust before it spreads out into the room. This definition has been the cornerstone of various definitions of ventilation efficiency ever since.

The mathematical concepts of age and residence time were introduced in investigations of mixing characteristics in reactors by chemical engineers such as Danckwerts (1958) and Spalding (1958). They mentioned the similarity between the mixing of gases in reactors and the mixing of air in ventilated rooms. Sandberg (1981) first applied the concept of *age of air* to ventilation studies. He summarized various definitions of ventilation efficiency including relative efficiency, absolute efficiency, steady state efficiency, and transient efficiency. The sooner the supply air reaches a particular point in the room, the greater the air change efficiency at that point. This concept has been widely accepted by many researchers and organizations throughout the world including ASHRAE and AIVC.

The ASHRAE Handbook (2009) states that *ventilation effectiveness* is a description of an air distribution system's ability to remove internally generated pollutants from a building, zone, or space, whereas *air change effectiveness* is defined as a description of a system's ability to deliver ventilation air to a building, zone, or space. Thus, ventilation effectiveness indicates the effectiveness of exhaust, whereas the air change effectiveness indicates the effectiveness of supply. However, the terminology *ventilation effectiveness* commonly includes both supply and exhaust characteristics.

In this chapter, we provide a one-to-one analogy between exhaust effectiveness and supply effectiveness using the concept of the age of air. The meanings of local and overall values of supply and exhaust effectiveness need be understood appropriately in conjunction with the aforementioned definitions of ventilation effectiveness.

We also extend the theory of the local mean age of air and local mean residual lifetime of contaminant to a space with multiple inlets and outlets. Theoretical considerations are given to derive the relations between the LMAs from individual inlets and the combined LMA of total supply air. In addition, the relations between the LMRs toward individual outlets and the combined LMR of total exhaust air are considered. These relations can be used to investigate the effect of each supply inlet and/or the contribution of each exhaust outlet in a

space with multiple inlets and outlets. Three examples of tracer gas applications are included in this chapter.

2. Definitions of ventilation effectiveness

2.1 Age and residual-life-time

Consider a point P in a room with one supply air inlet and one return air exhaust. The *age of air* is the length of time required for the supply air to reach the point. As air can reach the point through various paths, the mean value of the ages at the point is called the *local mean age* (LMA) of the air at P. Likewise, the length of time required for the contaminant located at P to reach an exhaust is called the *residual lifetime of the contaminant* at P. The mean value through various paths is the *local mean residual lifetime* (LMR).

Local mean age represents the un-freshness of supply air so that it can be used as a local supply index at the point. Local mean residual lifetime represents the slowness of removal of the contaminant generated at the point, and can be used to represent a local exhaust index. The LMA and LMR represent the local supply and exhaust effectiveness, respectively, at the point in the room. We note that they depend on the room airflow pattern only, and should not be dependent on the source distribution of a contaminant in the space unless the contaminant concentration alters the airflow characteristics of the room.

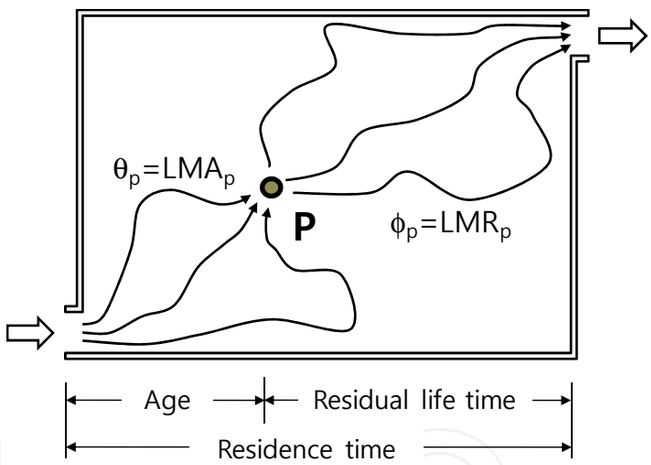


Fig. 1. Concept of age and residual lifetime of indoor air.

2.2 Supply and exhaust effectiveness

A complete mixing condition is considered to be a reference condition we can use to define ventilation effectiveness. The *air change rate* is the number of room volumes of air supplied in one hour, and is defined as Q/V where Q is the volumetric flow rate of air into the room and V is the room volume. The room *nominal time constant* τ_n is the inverse of the air change rate.

The local supply and exhaust indices are defined as the ratios of the local mean age and the local mean residual lifetime compared to the nominal time constant, respectively. These local indices can exceed 100% and can be as large as infinity.

Notice that the LMA at the exhaust means the total residence time of supply air in the space, which is the same as the LMR at the supply. We note that these values are equal to the nominal time constant.

$$\theta_{ex} = \phi_{\sup} = \tau_n \tag{1}$$

Therefore, the *local supply index* can be understood as the ratio of the LMA at the exhaust to that at the point, and the *local exhaust index* as the ratio of the LMR at the supply to that at the point. The overall room effectiveness can be defined similarly. The definitions of supply and exhaust effectiveness are shown in Table 1. The subscript P is the location of interest, and < > indicates the spatial average over the entire space.
It will be proved later in this chapter that the room averages of LMA and LMR are identical. Therefore, the overall room supply effectiveness and exhaust effectiveness should be the same. We do not need to distinguish the overall values, but we call this the *room ventilation effectiveness*. Note that supply effectiveness and exhaust effectiveness are meaningful only for local values.

SUPPLY EFFECTIVENESS	EXHAUST EFFECTIVENESS
Age of Air θ_P = Local Mean Age at P $<\theta>$ = Room Average of LMA	Residual Life Time of Air ϕ_P = Local Mean Residual Lifetime at P $<\phi>$ = Room Average of LMR
Local Supply Index $\alpha_p = \frac{\tau_n}{\theta_p} = \frac{\theta_{ex}}{\theta_P}$ = LMA at exhaust/LMA at P	Local Exhaust Index $\varepsilon_p = \frac{\tau_n}{\phi_p} = \frac{\phi_{\sup}}{\phi_P}$ = LMR at supply/LMR at P
Overall Room Supply Effectiveness $<\alpha> = \frac{\tau_n}{<\theta>}$	Overall Room Exhaust Effectiveness $<\varepsilon> = \frac{\tau_n}{<\phi>}$

Table 1. Definitions of supply and exhaust effectiveness using LMA and LMR

3. Tracer gas technique

3.1 Tracer gases

Tracer gas techniques have been widely used to measure air change rates and the air change effectiveness in a ventilated zone. Any measurable gas can be used as a tracer gas. It is desirable to follow air movements faithfully and for the gas to be nonreactive with other materials. Etheridge & Sandberg (1996) suggested that an ideal tracer gas should have the following characteristics:

- Not a normal constituent of the environment to be investigated.
- Easily measurable, preferably at low concentrations.
- Non-toxic and non-allergic to permit its use in occupied spaces.
- Nonreactive and non-flammable.
- Environmentally friendly.
- Economical.

A wide variety of gases have been employed as tracers. The characteristics of the most commonly used tracer gasses are given in Table 2. Carbon dioxide is a good tracer gas since it has a molecular weight similar to air and is mixed well with air. However, it has a background concentration of approximately 350 ppm, and it is produced by people and the

combustion of fuels in occupied spaces. The effect of the production should be compensated. Hydrogen gas and water vapor have also been also used as tracer gases by Dufton and Marley (1935). They pointed out problems related to phase change and adhesion on surfaces when using water vapor. Sulfur hexafluoride is also a common tracer gas used in various ventilated spaces. It is not present in normal ambient air and can be used at very low concentrations. This minimizes the amount of tracer gas needed for a test. However, it has a molecular weight approximately five times that of air, and it should be diluted and/or well mixed with the surrounding air during injection.

Gas	Molecular weight	Boiling point (˚C)	Density (15˚) (kg/m^3)	Analytical method	Detection range (ppm)	Background concentration	Toxicity
Carbon dioxide	44	-56.6	1.98	IR	0.05-2000	Variable	Slight
Freon12	121	-29.8	5.13	IR GC-ECD	0.05-2000 0.001-0.05		
Helium	4	-268.9	0.17	MS		5.24	
Nitrous oxide	44	-88.5	1.85	IR	0.05-2000	0.03	
Sulphur hexafluoride	146	-50.8	6.18	IR GC-ECD	0.05-2000 0.00002-0.5		
Perfluoron hexane	338	57.0		GC-ECD	10^{-8}		

Table 2. Characteristics of commonly used tracer gases (Sandberg, 1981)

3.2 Tracer gas system

A general tracer gas system is composed of an injection and distribution system, a sampling and monitoring system, and a data acquisition and control system. An example of a typical experimental setup is shown in Fig. 2 (ASTM, 1993).

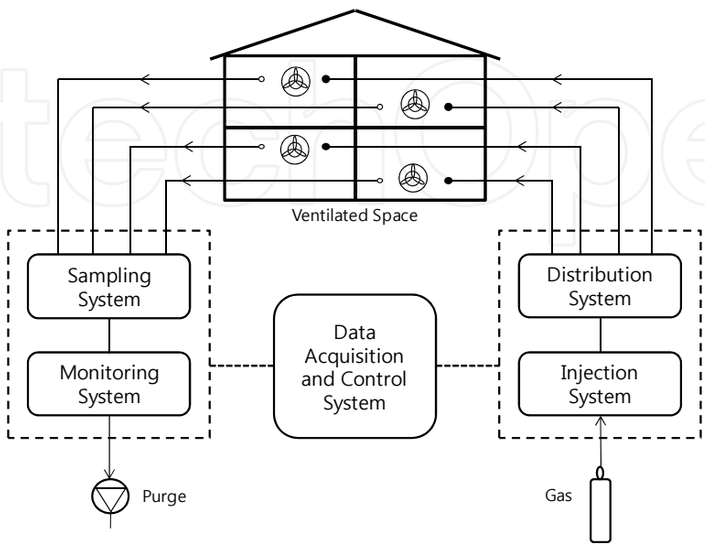


Fig. 2. Typical tracer gas experimental system.

3.2.1 Injection and distribution

The injection and distribution system releases an appropriate amount of tracer gas and distributes it into the zones. There are several means of releasing tracer gas, either manually or automatically. A graduated syringe or other containers of known volume may be used for simple manual injections. For automated injection systems, a compressed tracer gas supply is connected to a gas line with an electronic mass flow controller, or other tracer gas flow rate measurement and control devices.

An automatic distributing system includes a tubing network that dispenses a tracer gas via manifolds and automated valves, and pressure-operated valves that stop the flow from entering the tubing network when the tubing is not pressurized. There should be no leaks in the tubing. A mixing fan is frequently used for good mixing of tracer gases within a zone.

3.2.2 Sampling and monitoring

Air sampling can be achieved either manually or automatically. Manual samplers may include syringes, flexible bottles, or sampling bags with a capacity of at least three times the minimum sampler size of the gas analyzer used. Automatic samplers may utilize either a sampling network or automated samplers. Sampling networks consist of tubing, a manifold or selection switch that is typically solenoid-driven, and a pump that draws air samples through the network. Tracer gas molecules should not adhere to the tubing or manifold surfaces. Materials that absorb tracer gas may cause major inaccuracies in the measurement.

There are various types of gas analyzers based on principles such as infrared spectroscopy, gas chromatography, or mass spectroscopy. A gas analyzer should be suited to the tracer gas used, and the concentration range studied.

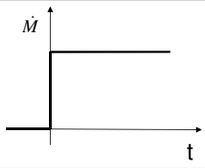
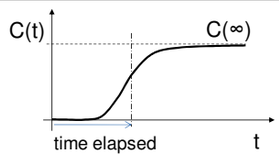
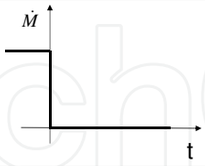
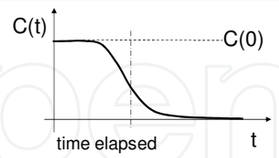
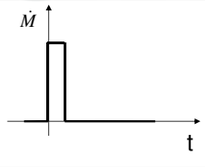
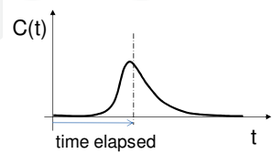
	INJECTION	MONITORING
Step-up method		
Step-down method		
Pulse method		

Table 3. Tracer injection methods and the corresponding concentration responses.

3.3 Tracer injection methods

There are three commonly used methods of injecting a tracer gas: step-up, step-down, and pulse methods. The *step-up method* introduces a tracer gas at a given time and onward until

it reaches a steady state. The concentration response at a monitoring point is observed continuously. As a steady state is reached, the concentration is maintained at the steady state value. The *step-down method* is the opposite of the step-up method. Tracer injection is stopped abruptly and the concentration decay is monitored at a monitoring point. The concentration decays exponentially and approaches a background concentration. The concentration decay method is frequently used to measure air change rate starting from a uniform mixing of room air. Finally, the *pulse method* introduces a certain amount of tracer gas in a short period of time. A peak concentration response is detected at a monitoring point with a time delay. The concentration decays down to an initial concentration after the peak. Table 3 shows concentration responses according to the three injection methods.

4. Measurements of ventilation effectiveness

4.1 LMA measurements

In order to measure the local mean age at point P, the tracer injection point should be at a supply diffuser and the monitoring point is at point P as shown in Fig. 3. LMA can be obtained by integrating the area above the concentration curve (shaded area) divided by the steady state concentration after a step-up tracer injection. Similarly, it is the area under the concentration curve for a step-down method. In the case of a pulse method, it can be calculated using the first moment of the area under the concentration curve. The equations used to calculate LMAs are shown in Table 4 for three injection procedures. The equations are different from one injection method to another, but the result should be the same. The superscripts and the subscripts of the concentrations indicate the injection and the monitoring points, respectively.

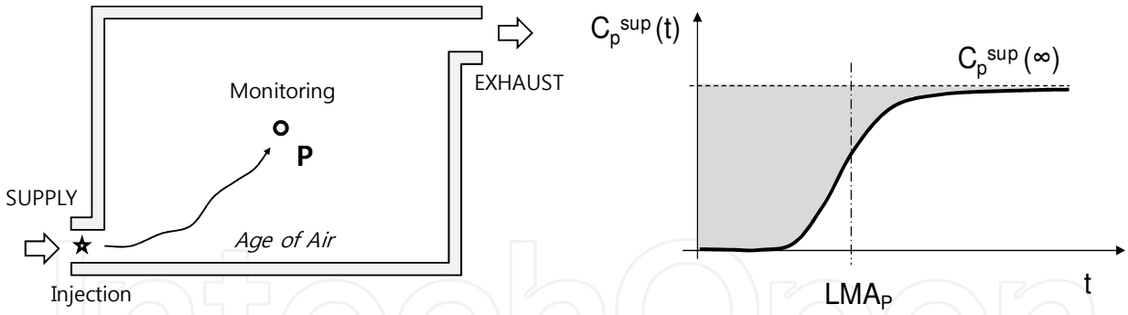


Fig. 3. Injection and monitoring points for LMA and transient step-up response.

It is known that the LMA distribution in a space is equivalent to the steady concentration distribution with uniformly-distributed sources in the space (Han, 1992). The proof is given in the appendix. Thus,

$$\theta_p = \frac{\overline{C}_p(\infty)}{\dot{m}} \tag{2}$$

where $\dot{m}$ is the tracer generation rate per unit volume. In Eq. (2), C has an over-bar rather than a superscript, which represents a uniform tracer injection throughout the entire space.
The local supply index, which is the ratio of the LMAs at the exhaust and at P, is calculated using the ratio of the steady concentrations with over-bars at those points. The steady

concentration at the exhaust can be obtained from the total tracer generation rate in the space, which is the product of the generation rate per volume times the space volume. Thus,

$$\alpha_p = \frac{\theta_{ex}}{\theta_P} = \frac{\overline{C}_{ex}(\infty)}{\overline{C}_p(\infty)} \tag{3}$$

	LOCAL MEAN AGE	LOCAL MEAN RESIDUAL-LIFE-TIME
Step-up	$\theta_p = \int_0^\infty \left(1 - \frac{{C_P}^{\sup}(t)}{{C_P}^{\sup}(\infty)}\right) dt$	$\phi_p = \int_0^\infty \left(1 - \frac{{C_{ex}}^{P}(t)}{{C_{ex}}^{P}(\infty)}\right) dt$
Step-down	$\theta_p = \int_0^\infty \frac{{C_P}^{\sup}(t)}{{C_P}^{\sup}(0)} dt$	$\phi_p = \int_0^\infty \frac{{C_{ex}}^{P}(t)}{{C_{ex}}^{P}(0)} dt$
Pulse	$\theta_p = \frac{\int_0^\infty t \cdot {C_P}^{\sup}(t) dt}{\int_0^\infty {C_P}^{\sup}(t) dt}$	$\phi_p = \frac{\int_0^\infty t \cdot {C_{ex}}^{P}(t) dt}{\int_0^\infty {C_{ex}}^{P}(t) dt}$

Table 4. Equations to calculate LMA and LMR for three injection methods

4.2 LMR measurements

In order to measure the local mean residual lifetime at P, the injection point should be at P and the monitoring point should be at the exhaust. The LMR can be obtained using the equations in Table 4 similar to LMA equations.

In a step-up method, the exhaust concentration reaches a steady state value ${C_{ex}}^{P}(\infty)$ as time goes to infinity. The mass balance should be satisfied; thus, the steady concentration at the exhaust should be equal to the total mass generation divided by the airflow rate, $\dot{M}/Q$. Therefore, the LMR using a step-up method can be written as

$$\begin{aligned} \phi_p &= \int_0^\infty 1 - \frac{{C_{ex}}^{P}(t)}{\dot{M}/Q} dt \\ &= \frac{1}{\dot{M}} \int_0^\infty \dot{M} - Q \cdot {C_{ex}}^{P}(t) dt \end{aligned} \tag{4}$$

where $\dot{M}$ is the contaminant generation rate at P. The first term in the integral is the total generation rate, and the second term is the rate of contaminant leaving the room through the extract duct. The integration of the difference up to the steady state results in the amount of contaminant left inside the room, which is called the *internal hold-up*. This is the product of the average room concentration times the room volume (Sandberg, 1981). Then, Eq. (4) can be written as

$$\begin{aligned} \phi_p &= \frac{< C^P(\infty) > V}{\dot{M}} \\ &= \frac{< C^P(\infty) > \tau_n}{{C_{ex}}^{P}(\infty)} \end{aligned} \tag{5}$$

The local exhaust index can be obtained either from the definition of the LMR ratio, or by the ratio of the room average concentration to the exhaust concentration when a source is located at P. Thus,

$$\varepsilon_p = \frac{C_{ex}{}^p(\infty)}{< C^p(\infty) >} \tag{6}$$

Equation (6) looks quite similar to the classical definition by Yaglou and Witheridge (1937). They also defined ventilation efficiency as the ratio of the room average concentration to exhaust concentration for a given contaminant source. They understood this quantity as the overall efficiency of the room, not as a local efficiency at the given source location, though. The ratio shown in Eq. (6) is not the room exhaust index, but the local exhaust index for a given source located at P. Various definitions have been proposed for removal effectiveness by several authors (Sandberg and Sjoberg, 1983; Skaaret ,1986). Although there have been many studies on the measurement of LMA (Shaw *et al*., 1992; Han *et al*., 1999; Xing *et al*., 2001), the distributions of LMR have rarely been measured experimentally (Han *et al*., 2002).

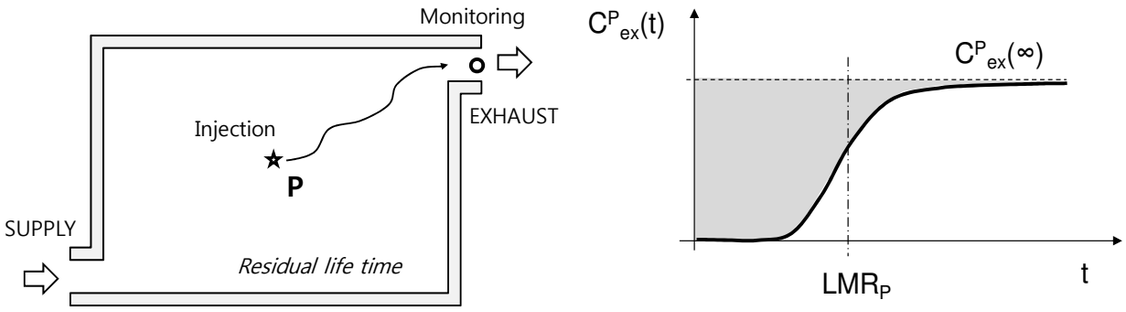


Fig. 4. Injection and monitoring points for LMR and transient step-up response.

4.3 Overall ventilation effectiveness

The overall room effectiveness is the spatial average of local values over the entire space. As previously discussed, LMA can be obtained using transient and steady approaches. The steady method indicates that the spatial average of LMA is the spatial average of the steady concentration distribution with uniformly distributed tracer sources of unit strength, as follows:

$$< \theta >= \frac{< \overline{C}(\infty) >}{\dot{m}} \tag{7}$$

Therefore, the overall supply effectiveness; i.e., the ratio of LMA at exhaust to the room average LMA, equals the ratio of the concentration at exhaust to the spatial average of the steady concentration as follows:

$$< \alpha >= \frac{\overline{C}_{ex}(\infty)}{< \overline{C}(\infty) >} \tag{8}$$

On the other hand, to obtain the overall exhaust effectiveness, LMR should be obtained at every internal point to calculate its spatial average over the entire space. Unlike the method

used for LMA measurements, a monitoring point should be fixed at the exhaust, and a tracer should be injected at every point in the space repeatedly. The concentration response by simultaneous tracer injections can be obtained by superimposing every injection source present over the entire space, since the concentration equation is linear. Therefore, the room average exhaust effectiveness is the ratio of the exhaust concentration to the room average concentration with a uniformly distributed source superimposed in the space, which is identical to the steady method used to determine overall supply effectiveness. This concludes the proof that supply effectiveness equals the overall exhaust effectiveness of a given space, and that the room mean age of air is identical to the room mean residual lifetime:

$$<\varepsilon>=<\alpha> \tag{9}$$

The room mean age or the room mean residual lifetime can also be obtained from the transient concentration responses at exhaust according to Table 5 for different tracer injection methods (Kuehn *et al*., 1998).

	ROOM MEAN AGE = ROOM MEAN RESIDUAL-LIFE-TIME
Step-up method	$<\theta>=<\phi>=\frac{Q}{V}\int_0^\infty t\cdot\left(1-\frac{C_{ex}{}^{\sup}(t)}{C(\infty)}\right)dt$
Step-down method	$<\theta>=<\phi>=\frac{Q}{V}\int_0^\infty t\frac{C_{ex}{}^{\sup}(t)}{C(0)}dt$
Pulse method	$<\theta>=<\phi>=\frac{Q}{2V}\frac{\int_0^\infty t^2\cdot C_{ex}{}^{\sup}(t)dt}{\int_0^\infty C_{ex}{}^{\sup}(t)dt}$

Table 5. Equations used to calculate RMA and RMR for three injection methods

5. Multiple inlets and outlets

5.1 LMA from multiple inlets

When there are multiple supply inlets, the LMA from one inlet is different than those from the other inlets. Consider a ventilated space configuration with two supply inlets as shown in Fig. 5. The airflow rates through the inlets are Q_a and Q_b, respectively, and room air is exhausted through an outlet on the other side of the space.

Suppose we inject a tracer gas only at inlet ***a*** by a step-up method. The supply concentration is assumed to be 1.0 at inlet ***a*** and 0.0 at inlet ***b***. The concentration response at P, $C_P{}^a(t)$, is shown in Fig. 5. $LMA_P{}^a$ is the area above the curve (left-hatched area). Subscript P represents a monitoring point, and superscript ***a*** represents an injection location. The steady concentration $C_P{}^a(\infty)$ has a value ranging between zero and unity because the supply concentration at inlet ***a*** is non-dimensionalized.

The response after a step-up injection at inlet ***b*** can be characterized similarly by $LMA_P{}^b$ and $C_P{}^b(\infty)$. In this case, the non-dimensional supply concentration is 0.0 at inlet ***a*** and 1.0 at

inlet ***b***. We note that the steady state concentration $C_P{}^b(\infty)$ is complementary to $C_P{}^a(\infty)$, since the inlet concentration boundary conditions are switched.
In the case of simultaneous tracer injections at both inlets, the concentration response at point P is given by the addition of the concentration responses from individual injections, as shown in Fig. 5.

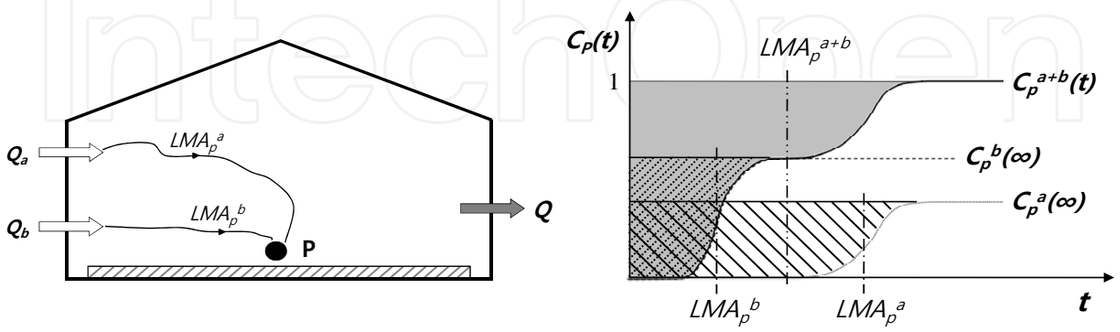


Fig. 5. Local mean age from individual supply inlets and concentration responses at P.

$$C_P{}^{a+b}(t) = C_P{}^a(t) + C_P{}^b(t) \tag{10}$$

This is because the indoor airflow pattern remains unchanged and the governing equation is linear with respect to concentration. Concentrations reach 1.0 at all internal points as a steady state is reached. Thus,

$$1 = C_P{}^a(\infty) + C_P{}^b(\infty) \tag{11}$$

The combined LMA is the area above the combined concentration curve, which is the shaded area in Fig. 5. The relations between the LMAs can be derived as follows (Han *et al.*, 2010):

$$LMA_P = C_P{}^a(\infty) \cdot LMA_P{}^a + C_P{}^b(\infty) \cdot LMA_P{}^b \tag{12}$$

Therefore, the combined LMA is the weighted average of the LMAs from each individual inlet, and the weighting factors for calculating the average are the corresponding steady state concentrations at the point. The steady state concentrations can be considered to be the contribution factors of the corresponding inlets for characterizing the supply air conditions at the point.

5.2 LMR to multiple outlets

If there are multiple outlets, the contribution of each outlet is different with respect to eliminating contaminants generated in a space, depending on the relative source locations. Consider a case with two outlets with exhaust flow rates of Q_a and Q_b as shown in Fig. 6. The time for the contaminant generated at P to reach one exhaust, $LMR_P{}^a$, is different from the time to reach the other, $LMR_P{}^b$. The total amount of contaminants exhausted by one outlet is different from that exhausted by the other. Figure 6 shows concentration responses at the exhausts according to a step-up injection at point P. The combined exhaust

concentration is the average of individual exhaust concentrations weighted by the airflow rates through the outlets, as follows:

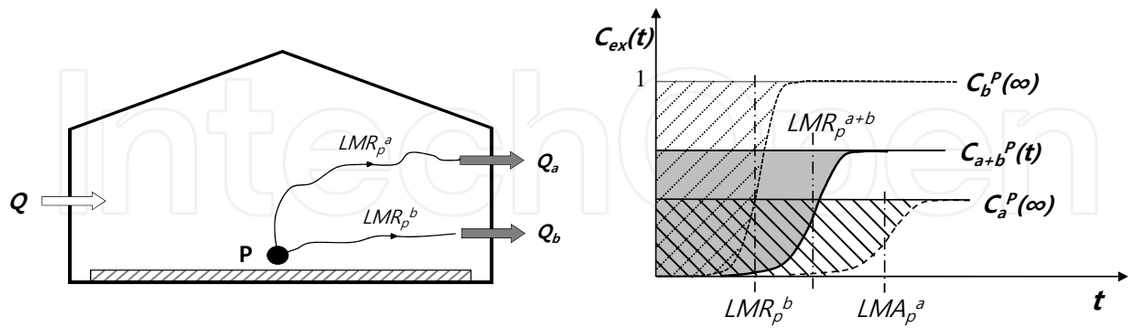


Fig. 6. Local mean residual lifetime at P and concentration responses at the exhausts.

$$C_{ex}(t) = \frac{Q_a}{Q} C_a{}^P(t) + \frac{Q_b}{Q} C_b{}^P(t) \tag{13}$$

The individual LMRs to the outlets can be obtained by integrating the areas above the corresponding concentration curves:

$$\begin{aligned} LMR_P{}^a &= \int_0^\infty 1 - \frac{C_a{}^P(t)}{C_a{}^P(\infty)} dt \\ LMR_P{}^b &= \int_0^\infty 1 - \frac{C_b{}^P(t) dt}{C_b{}^P(\infty) dt} \end{aligned} \tag{14}$$

Similarly, the combined LMR can be obtained by the area above the average exhaust concentration curve. The combined LMR can be rearranged using Eq. (13), and can be expressed with the individual LMRs as follows:

$$\begin{aligned} LMR_P &= \int_0^\infty 1 - \frac{C_{ex}(t)}{C_{ex}(\infty)} dt \\ &= \int_0^\infty \frac{\left(\frac{Q_a}{Q} C_a{}^P(\infty) + \frac{Q_b}{Q} C_b{}^P(\infty) \right) - \left(\frac{Q_a}{Q} C_a{}^P(t) + \frac{Q_b}{Q} C_b{}^P(t) \right)}{C_{ex}(\infty)} dt \\ &= \frac{C_a{}^P(\infty) Q_a}{C_{ex}(\infty) Q} \cdot LMR_P{}^a + \frac{C_b{}^P(\infty) Q_a}{C_{ex}(\infty) Q} \cdot LMR_P{}^b \\ &= \frac{\dot{M}_a}{\dot{M}} \cdot LMR_P{}^a + \frac{\dot{M}_b}{\dot{M}} \cdot LMR_P{}^b \end{aligned} \tag{15}$$

Therefore, the combined LMR is the weighted average of the individual LMRs. The weighting factors are the percentages of the contaminant removal rates through the corresponding exhaust outlets. They can be understood as the contribution factors of the individual outlets for a given tracer source at P.

6. Examples of tracer gas applications

6.1 Effect of supply air temperature on LMA distributions

6.1.1 Problem description

It is often observed that fresh air supplied to a space is bypassed directly to an exhaust without contributing to effective room ventilation. Bypass affects the ventilation effectiveness of the room significantly. It is quite common in office buildings, especially when warm air is supplied from ceiling diffusers in the winter season. The following example considers the effect of supply air temperature on LMA distribution in a rectangular space with a diffuser and a return grill on the ceiling.

6.1.2 Experimental setup

A schematic of the experimental chamber is shown in Fig. 7. The chamber measures 1.95 m × 1.95 m × 1.45 m. The height of 1.45 m is about one-half of a full-scale office room. The interior surfaces (walls and floors) are made of aluminum panels. By circulating temperature-controlled fluid through the passages embedded in each panel, the temperatures of the walls and floors are precisely controlled. The ceiling is insulated with polystyrene insulation boards of 50 mm thickness. Air is supplied to the chamber through three linear sections that measures 0.635 m in length and 0.0508 m in width each. The three sections are aligned to form a 0.0508 m × 1.905 m straight slot inlet in the ceiling. The return slot is identical to the inlet and is also placed in the ceiling. This configuration produces a two-dimensional (2-D) flow in the chamber. A detailed description of the physical structure and the control system of the chamber is given by Corpron (1992).

6.1.3 Similitude

In this study, The Reynolds number and Archimedes number are considered important in simulating the full-scale conditions. These dimensionless numbers are defined as follows:

$$\mathrm{Re} = \frac{\rho u L}{\mu} \quad \propto \quad \frac{inertia\ force}{viscous\ force} \tag{16}$$

$$\mathrm{Ar} = \frac{\beta g L \Delta T}{u^2} \quad \propto \quad \frac{buoyancy\ force}{inertia\ force} \tag{17}$$

For a half-scale model, the characteristic length is related as $L_m = N\,L_f$, where N equals 0.5. Subscript m stands for the model and f represents the full scale. As the thermodynamic properties ρ, μ, and β are assumed to be constant for both, the characteristic velocity of the model needs to be increased by a factor of $1/N$. Also, the temperature difference needs to be increased by a factor of $1/N^3$ for similarity. Thus,

$$u_m = \frac{1}{N} u_f \tag{18}$$

$$(\Delta T)_m = \frac{1}{N^3} (\Delta T)_f \tag{19}$$

The air change per hour (ACH) is the ratio of volumetric flow rate to the volume of the room. By a simple mathematical manipulation, the relation of ACH between the model and the prototype becomes

$$(ACH)_m = \frac{1}{N^2}(ACH)_f \tag{20}$$

6.1.4 Experimental procedure

The airflow and temperature conditions of the chamber were adjusted and checked until the steady state was reached. The sampling tube was positioned at a monitoring point using the three-dimensional (3-D) traversing system. Using a syringe, 3 mL of SF_6 gas was injected into the supply duct. The gas monitor started to take data at the same time as the gas injection, which works on the principle of electron capture gas chromatography. Concentration data were recorded every 70 s until the concentration fell within 1% of the maximum concentration. The same measurement was repeated with a delayed injection by 35 s to double the number of data points. The sampling port was then moved to the next position, and the aforementioned procedure was repeated to cover the entire cross-section at the center of the chamber.

In order to investigate the effect of thermal buoyancy, three different temperature conditions were tested: isothermal, cooling, and heating. The experimental conditions and measurements are summarized in Table 6. The values of the corresponding full scale situation are shown in parentheses.

	Isothermal	Cooling	Heating
Pressure drop across nozzle [mmH_2O]	17.5	11.2	22.5
Supply velocity at diffuser [m/s]	1.032	0.813	1.209
Supply airflow rate [m^3/h]	345	272	404
Air change per hour [ACH]	62.6 (15.6)	49.4 (12.4)	73.3 (18.3)
Supply air temperature [°C]	24.4 (24.4)	-1.6 (19.2)	57.1 (30.5)
STD of supply air temperature [°C]	0.1	1.2	1.9
Exhaust air temperature [°C]	24.4 (24.4)	27.6 (22.9)	41.4 (28.5)
Wall temperature [°C]	24.4 (24.4)	46.0 (25.2)	-3.7 (22.9)
STD of wall temperature [°C]	0.1	4.4	2.2
Ceiling temperature [°C]	24.4 (24.4)	24.3 (22.5)	23.4 (26.3)
Mean temperature [°C]	24.4	22.2	26.7
$T_{wall} - T_{supply}$ [°C]	0 (0)	47.6 (6.0)	-60.8 (-7.6)
Reynolds number	3374	3128	3293
Archimedes number	0	0.1215	-0.0690

*Numbers in ( ) indicate the corresponding values in full-scale situations.

Table 6. Experimental conditions and measurements (Han, 1999)

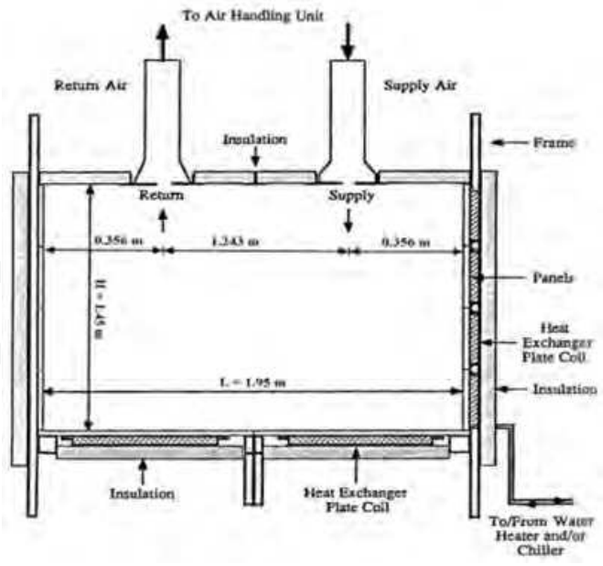


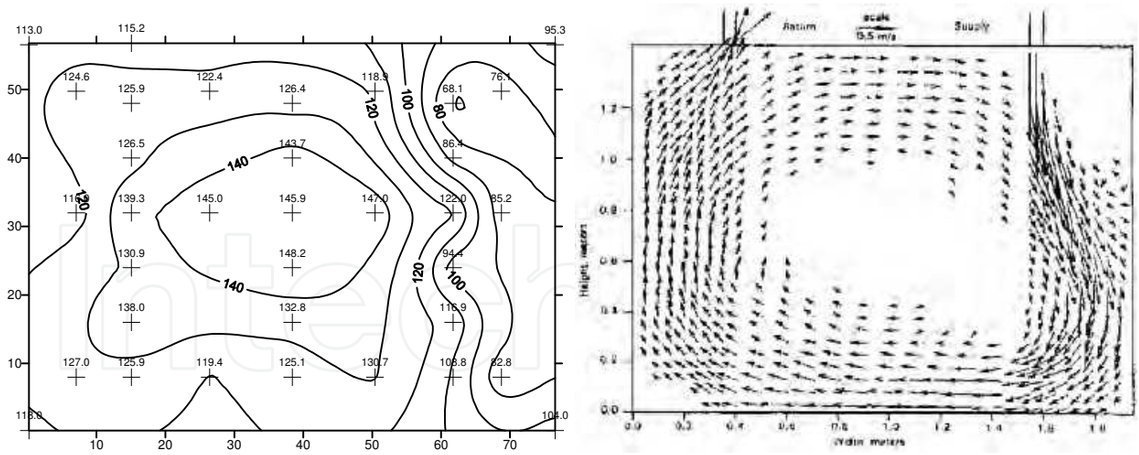
Fig. 7. Cross-section of a thermal chamber (Han, 1999).

6.1.5 Results and discussion

Figure 8 shows LMA contours superimposed with the LMA data measured at 36 locations for an isothermal condition. The LMA distribution is nearly uniform over the entire cross-section except at corners. The maximum LMA was observed at the center, which indicates there is a large recirculation in the middle of the chamber. A velocity vector drawing by Liang (1994) is also shown in Fig. 8. The air jet from the supply inlet moves downward and leaves the chamber through the exhaust after making a large clockwise circulation in the space. The supply jet is attached to the right wall, and then separates before it hits the floor. This tendency for flows to attach to walls is known as the Coanda effect. It is interesting to note that the distribution of local mean age in the space shows a good overall picture of the airflow pattern in the space.

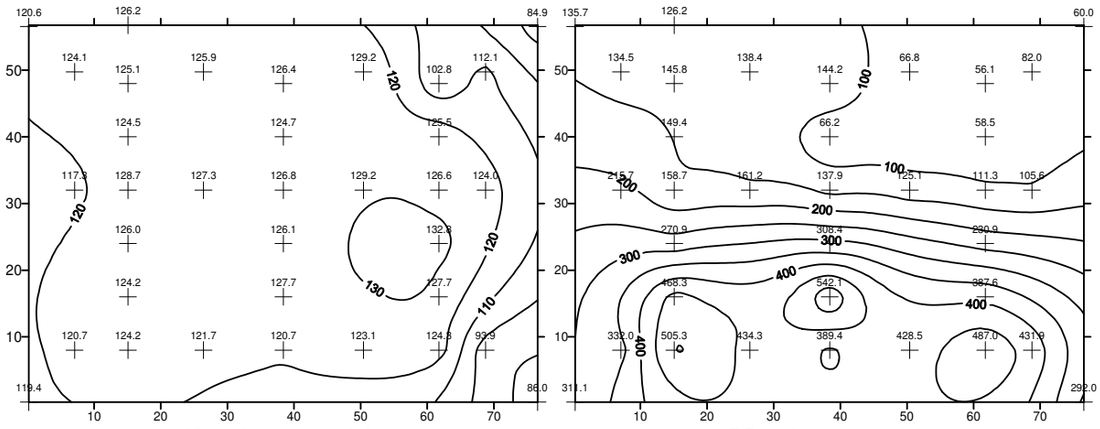
For a cooling condition, the supply air temperature is lower than the room temperature and the buoyant force acts downward, which is the same as the direction of the supply air. Figure 9(a) shows the LMA distribution in the chamber. Assisted by buoyancy, the mixing of the flow is enhanced and the local mean age values are more uniformly distributed compared to the isothermal condition. The location of maximum LMA is shifted downward and to the right in comparison with the isothermal condition. The maximum LMA value is less than that in the isothermal case.

In a heating condition, the thermal buoyancy opposes the inertial effect. The local mean age distribution is shown in Fig. 9(b). A large variation in LMA can be observed in the chamber because of thermal stratification. The variation is small at the upper part and large at the lower part of the chamber. The air jet from the supply port does not seem to penetrate into the space effectively; rather, it short circuits to the exhaust duct. Liang (1994) observed that the flow field under the heating condition was unstable and the supply jet oscillated slowly within the chamber. Because of the oscillatory behavior, velocity vectors could not be measured in the experiment, and only the frequency of the oscillatory motion was reported. The room mean ages obtained by integrating the local mean age values over the entire space give 118 s, 120 s, and 234 s for the isothermal, cooling, and heating conditions, respectively.



(a) LMA distribution (Han, 1999). (b) Velocity vectors (Liang, 1994).

Fig. 8. LMA distribution and velocity vector fields for isothermal condition.



(a) Cooling condition. (b) Heating condition.

Fig. 9. Local mean age distributions for cooling and heating conditions (Han, 1999).

6.1.6 Concluding remarks

Using a pulsed injection method using SF_6 tracer gas, LMA distributions were measured in a half-scale thermal chamber. Boundary conditions were applied that simulated isothermal, heating, and cooling conditions by controlling the supply air temperature and the wall temperature.

1. The LMA distribution was found to be closely related to the velocity distribution in the chamber. The results for LMA distributions are in good agreement qualitatively with the velocity patterns obtained by Liang (1994).
2. For an isothermal condition, the largest LMA occurred at the center and not at the corners, which indicates that there was a large recirculating zone at the center. During a cooling operation, supply air penetrated deeply into the chamber, and mixing was enhanced compared to the isothermal condition.
3. For a heating condition, there was a large variation of local mean ages due to thermal stratification in the chamber. It can be concluded that local ventilation effectiveness in the lower part of a room can be very poor under heating operations.

Further research needs to be done to improve the tracer gas technique and to apply the technique to various applications.

6.2 Effect of inlet/outlet configurations on LMA and LMR distributions

6.2.1 Problem description

The airflow pattern in a ventilated space varies according to the locations of supply inlets and exhaust outlets. In this example, LMA and LMR distributions are measured and compared in a rectangular enclosure with three different inlet/outlet configurations. A supply slot is fixed at the top of a right wall, and an exhaust slot is varied at the bottom-left (Case 1), bottom-right (Case 2), and top-left (Case 3) locations.

6.2.2 Experimental setup

The experimental chamber has dimensions of 1.8 m x 1.2 m x 0.9 m. There is a supply slot on the top of the right wall, and an exhaust slot at one of the three locations. The supply and exhaust slots are 0.025 m in width, and supply air was discharged horizontally. The airflow rate ranged from 4 to 76 ACH. The pressure inside the chamber was maintained neutral by an exhaust fan in order to minimize infiltration through the envelope. Sulfur hexafluoride at 30% concentration was used as a tracer gas. Using a syringe, 10 mL of SF_6 was injected into a polystyrene tube, and the gas was mixed with a continuous stream of nitrogen. The diluted tracer gas was discharged at a point in the chamber through a porous sphere 40 mm in diameter connected at the end of the injection tube. A tracer gas detector is a multi-gas monitor based on the non-disperse infrared (NDIR) absorption principle. To visualize airflow patterns in the chamber, helium bubbles were discharged into a supply air duct, and a sheet of light was illuminated through a glass window along the center of the chamber. A schematic diagram of the experimental setup is shown in Fig. 10.

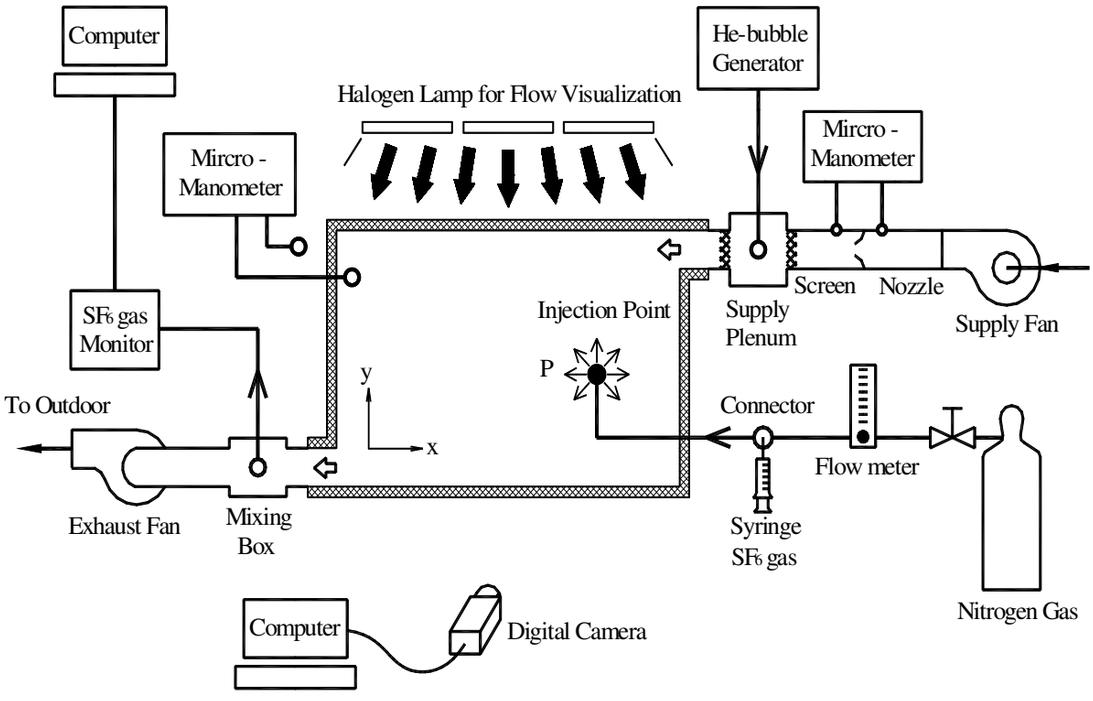


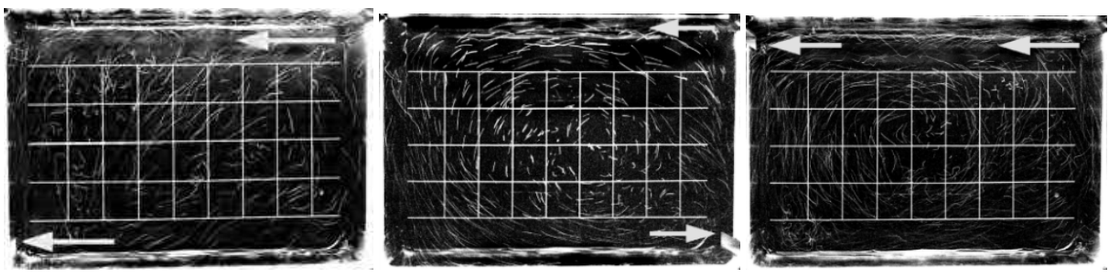
Fig. 10. Schematic diagram of experimental setup (Han *et al*., 2002).

6.2.3 Experimental procedure

For the LMR measurements, tracer gas was injected through a porous sphere at a point in the chamber and the transient tracer gas concentration variation was measured at the exhaust. After the tracer gas was exhausted completely from the chamber, the injection sphere was moved to another position. The procedure was repeated for other internal points. There are 15 injection points equally spaced in the center plane of the chamber.
For LMA measurements, all the experimental conditions were identical to the LMR case, but tracer gas was injected at a supply duct. Then, transient tracer gas concentration variation was measured at the internal points. Experiments were conducted for three different exhaust locations under isothermal room temperature conditions.

6.2.4 Results and discussion

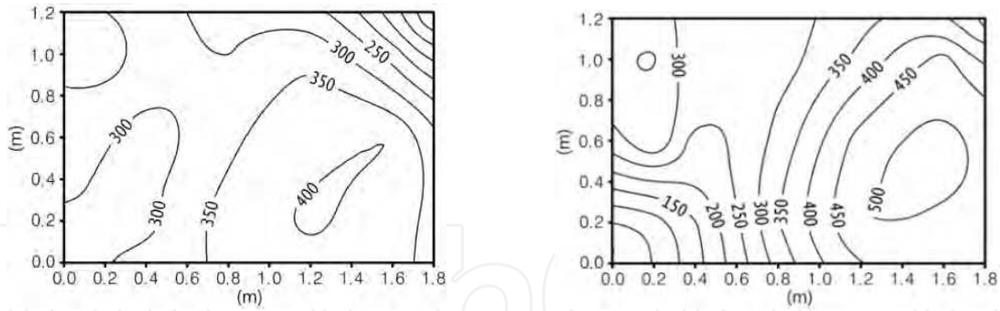
Flow visualization results are shown in Fig. 11 for three different exhaust locations. The air change rates are 12ACHs. For Case 1, the air supplied in the horizontal direction moved toward the lower-left exhaust in the diagonal direction. The room air formed two large recirculating flows at the upper-left and lower-right corners. For Case 2, the air supplied along the ceiling changed its direction by the opposite wall and made a large counter-clockwise circulation in the chamber. We note that the airflow pattern was quite similar to a complete mixing condition. For Case 3, supplied air faced directly toward the exhaust. The room air was mostly stagnant, but with a slow recirculation due to the viscous action of the bypassing flow along the ceiling.



(a) Case 1 (b) Case 2 (c) Case 3

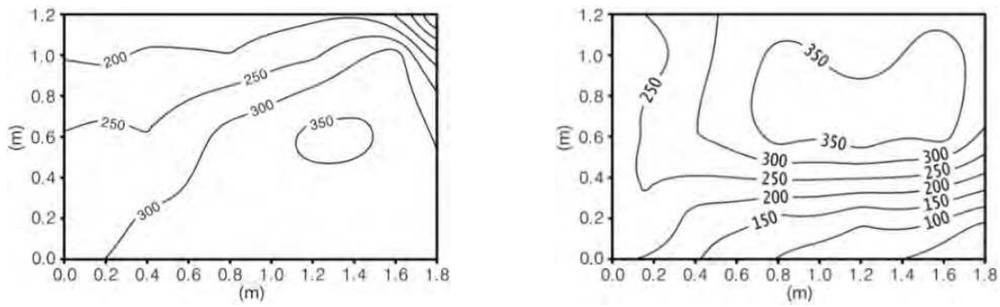
Fig. 11. Flow visualization results for three inlet-outlet configurations.

Contours of LMA and LMR are plotted in Fig. 12 for Case 1. It can be seen that both of the distributions are closely related to the airflow pattern shown in Fig. 11(a). LMA and LMR values are large within recirculating zones. LMA is small adjacent to the supply inlet and large adjacent to the exhaust, whereas LMR is small adjacent to the exhaust and large adjacent to the supply inlet. Figure 13 shows LMA and LMR distributions for Case 2. The LMA near ceiling is relatively small, whereas the LMR near floor is small. Both have large values within a large recirculation zone at the center. Figure 14 shows the results for Case 3. The LMA and LMR are small near ceiling, and large adjacent to the floor. The airflow pattern in Fig. 11(c) indicates there was large stagnant recirculation in the lower part of the space. The tracer gas diffused out into the lower part could not be exhausted effectively.



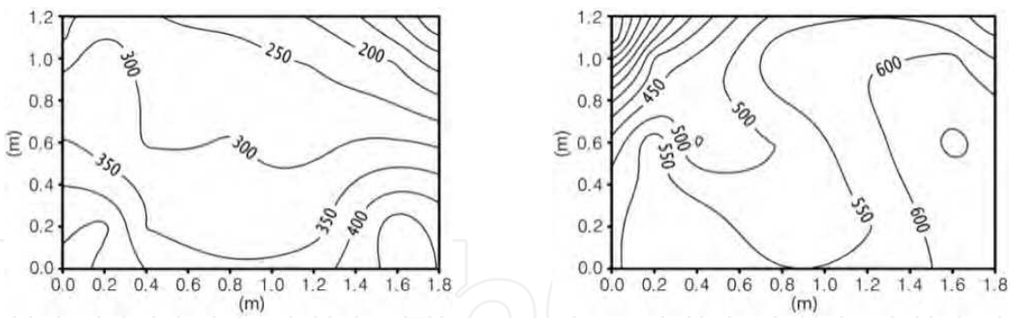
(a) LMA contour (s). (b) LMR contour (s).

Fig. 12. LMA and LMR distributions for Case 1 (Han *et al*., 2002).



(a) LMA contour (s). (b) LMR contour (s).

Fig. 13. LMA and LMR distributions for Case 2 (Han *et al*., 2002).



(a) LMA contour (s). (b) LMR contour (s).

Fig. 14. LMA and LMR distributions for Case 3 (Han *et al*., 2002).

Figure 15 shows room mean ventilation effectiveness for various air change rates. For Case 1, ventilation effectiveness decreased as the air change rate increased, but remained nearly constant for large air change rates over 20. It varies between 0.8 and 1.0, which is similar to a complete mixing condition. Note that the room ventilation effectiveness is 1 for complete mixing conditions, and 2 for perfect piston flow conditions. For Case 2, as the air change rate increased, the effectiveness increased initially and decreased slowly afterward. The effectiveness remained nearly constant for ACH over 20, similar to Case 1. However, the ventilation effectiveness in Case 3 is significantly lower compared to Cases 1 and 2, especially when the air change rate was low. This is due to the fact that the supply jet was not mixed well with the air in the chamber.

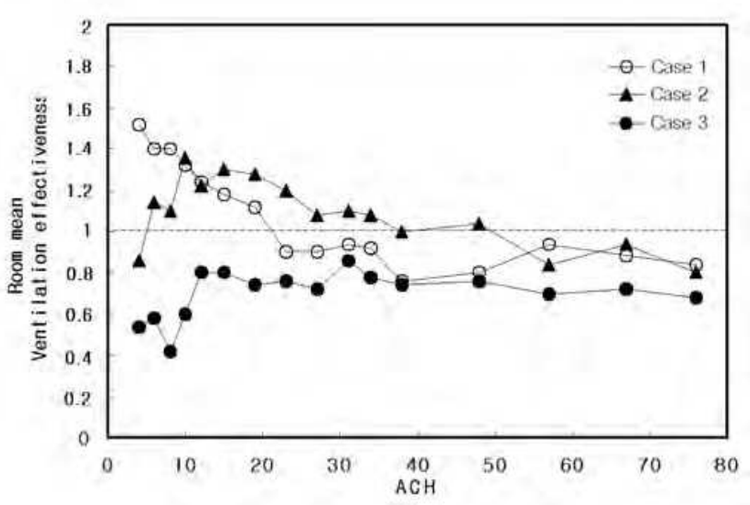


Fig. 15. Effect of air change rate on room mean ventilation effectiveness for three cases.

6.2.5 Concluding remarks

The distributions of LMA and LMR were obtained in a rectangular space with three different inlet and outlet configurations, and the corresponding airflow patterns were visualized.

1. The distributions of LMA and LMR show different characteristics, but both are closely related to the airflow pattern in the space.
2. LMA values are small adjacent to supply inlets, and large adjacent to return-air exhausts. LMR values are small adjacent to exhausts, and large adjacent to supply air inlets, as expected.
3. Compared to Cases 1 and 2, Case 3 shows poor overall room ventilation effectiveness, since the supply air jet is directed toward the exhaust outlet located at the opposite side.
4. The overall ventilation effectiveness depends not only on supply-exhaust configurations, but also on the air change rate.

The concept of local mean residual lifetime of the contaminant can be used in designing the layouts of exhausts and contaminant sources in a building such as a smoking zone, whereas concept of local mean age can be used in designing a proper distribution of fresh supply air into an occupied zone.

6.3 LMA distributions in a space with multiple inlets

6.3.1 Problem description

A space with multiple inlets is considered. It has a pentagonal shape with two inlets and a single outlet, which models a simplified livestock building. The LMAs from individual inlets are obtained by injecting a tracer gas at each inlet separately, and the combined LMA is obtained by injecting a tracer gas at both inlets simultaneously. This example is intended to verify the relation previously derived theoretically between the LMAs.

6.3.2 Experimental setup

The experimental chamber is pentagonal in shape with a height of 1.4 m and a width of 3.0 m. It is roughly a one-third scale model of a livestock building. The chamber has a length of 0.15

m, and thus can be considered 2-D. There are five openings in the model, and three are used for our experiment. Two openings on the left wall (vents ***a*** and ***b***) are used as supply inlets, and one opening on the opposite wall (vent ***d***) is used as an exhaust. Vents that are not used for the experiment have been carefully sealed. The sizes of all openings are 0.05 m x 0.15 m. A schematic diagram of the experimental setup is shown in Fig. 16.

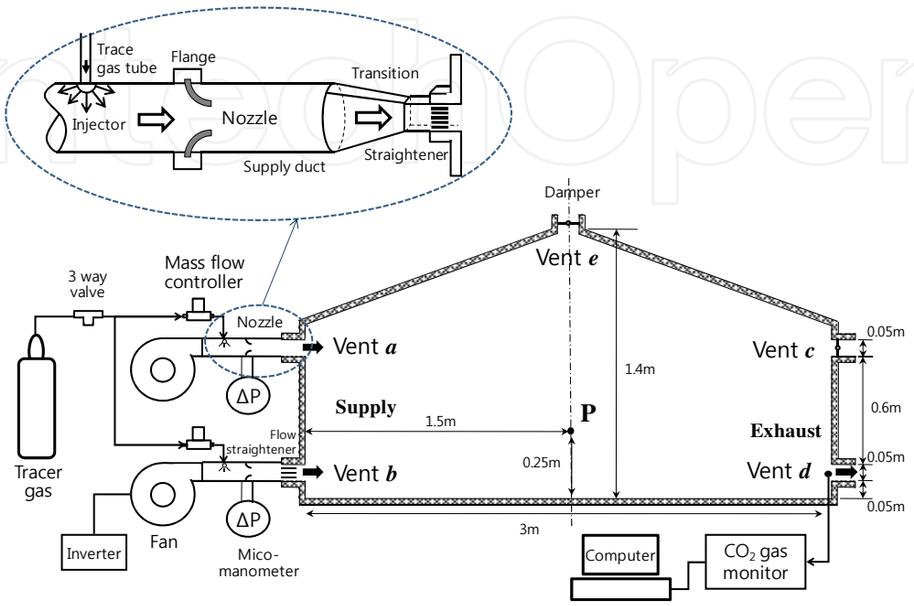


Fig. 16. Schematic diagram of experimental setup (Han *et al.,* 2011).

Carbon dioxide was used as a tracer gas. Injection ports were installed in both supply ducts upstream of the flow nozzles to ensure that the tracer gas was well mixed with incoming air streams. The amount of tracer gas was controlled by mass flow controllers (MFCs). A MFC contains a thermal mass flow meter that measures the air temperature rise across an internal heater. The range is between 0 and 10 L/min, and the error is reported to be below 1% of the measured values. A step-up method was adopted for tracer injection using a MFC. The tracer gas injection rate was held constant until a steady state condition was reached. The gas detector was an infrared single gas analyzer, and the sampling interval was 1.6 s. The range of the monitor was 20,000 ppm maximum, and the accuracy is 1% of the range.

6.3.3 Experimental procedure

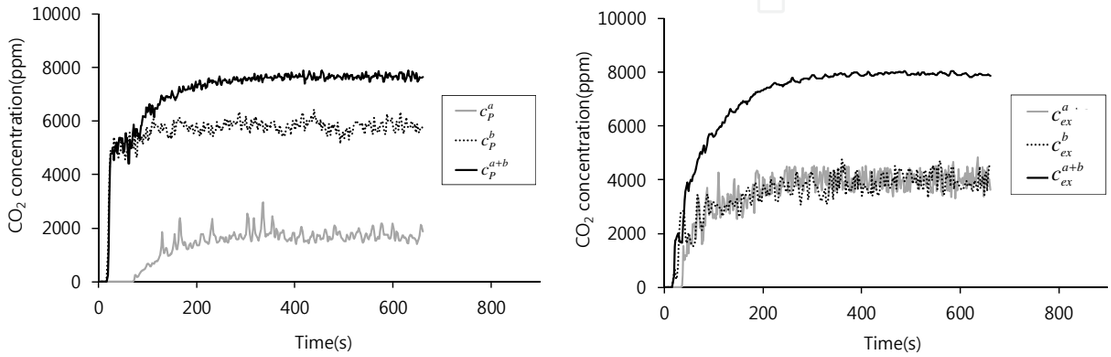
Three cases of tracer injections were applied: injection at vent ***a***, injection at vent ***b***, and injection at vents ***a*** and ***b*** simultaneously. In order to obtain local mean age distributions in the space, tracer concentration responses were measured at 19 internal points evenly distributed in the space, including point P. The airflow rate was varied from 16.2 to 54 CMH. The airflow rates of vents ***a*** and ***b*** are maintained to be the same.

6.3.4 Results and discussion

Figure 17 shows concentration responses measured at point P and at the exhaust. The concentrations have been obtained by subtracting the background concentration, which is the average concentration measured before a tracer injection is applied. The total airflow

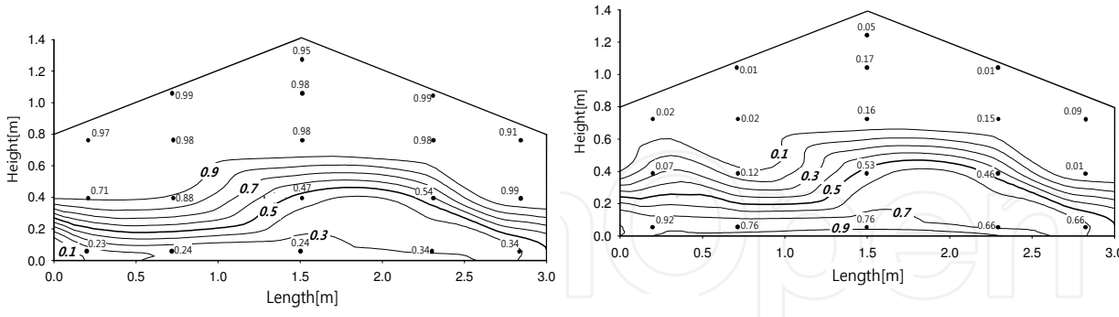
rate was 27 CMH. Each figure shows three injection cases: injection at vent ***a*** (Case ***a***), at vent ***b*** (Case ***b***), and at vents ***a*** and ***b*** (Case ***c***).

The concentrations increased rapidly initially, and reached a constant steady state. The steady concentrations indicate the effective supply airflow rates contributing to the ventilation at the point by each supply inlet in a relative sense. The steady concentration in Case ***b*** is greater than that in Case ***a***, which means the ventilation performance at point P was influenced more by the supply air from vent ***b*** than by the supply air from vent ***a***. At the exhaust, the steady concentrations in Cases ***a*** and ***b*** are nearly the same, since the airflow rates of the two inlets are the same. We note that the non-dimensional steady concentrations at the exhaust could be determined by the relative airflow rates from the two supply inlets.



(a) At point P. (b) At exhaust.

Fig. 17. Concentration responses at P and at exhaust after step-up injections at the inlets (Han *et al.,* 2011).



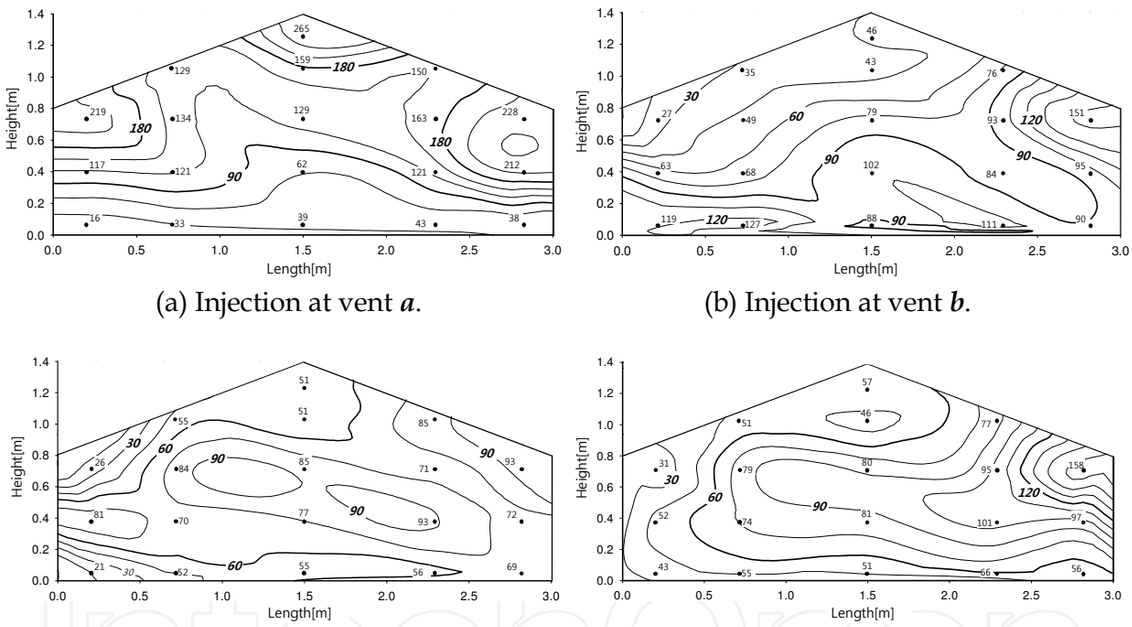
(a) Injection at vent ***a***. (b) Injection at vent ***b***.

Fig. 18. Spatial distributions of steady concentrations (Han *et al.,* 2011).

The steady concentrations were obtained by taking the averages of the fluctuating concentrations for a certain period of time after reaching the steady state. Figure 18 shows the spatial distributions of the steady concentrations measured at internal points. The concentration values have been made dimensionless by dividing those by the steady concentrations obtained in Case ***c***. Iso-concentration contours were drawn based on the numerical values measured at the grid points. In Fig. 18(a), non-dimensional steady concentrations by vent ***a*** are greater than 0.5 at an upper part of the space, and less than 0.5

at a lower part of the space. The concentration distributions by vent ***b*** are the opposite, as shown in Fig. 18(b). The non-dimensional steady concentrations are complimentary to each other; i.e., the sum of the concentrations is unity at any point in the space.

LMA contours from individual inlets are shown in Fig. 19. Figure 19(a) shows small LMAs in the vicinity of vent ***a***, and large LMAs near vent ***b*** and at the upper-right corner. Figure 19(b) shows small values starting from vent ***b*** along the floor up to the exit on the right, and large values at three corners in the upper part of the space. By following the contour lines, we can visualize the approximate airflow pattern in the space directed toward the exit. Figure 19(c) shows the combined LMA by simultaneous injections at both supply inlets. The LMAs are small along the floor near vent ***a***, and along the left part of the roof near vent ***b***. The combined LMA can be calculated from the individual LMAs according to Eq. (12). The distribution is shown in Fig. 19(d) and can be compared to Fig. 19(c). The overall patterns are in good agreement.



(a) Injection at vent ***a***. (b) Injection at vent ***b***.

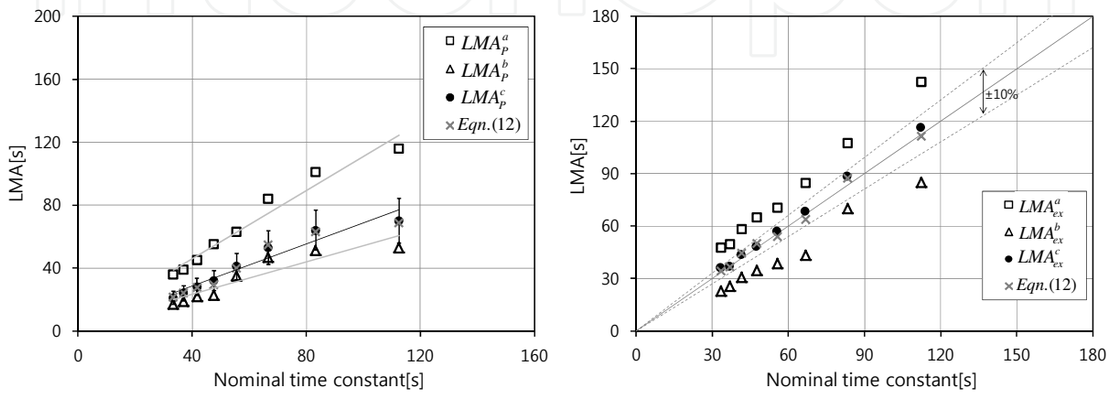
(c) Simultaneous injection at vents ***a*** and ***b.*** (d) Weighted average of (a) and (b).

Fig. 19. Spatial distributions of local mean ages for Cases ***a***, ***b***, and ***c,*** with weighted averages (Han *et al.,* 2011).

The local mean ages at P are shown in Fig. 20(a) for various airflow rates. The airflow rate is expressed with the nominal time constant, which is the inverse of the air change rate. As the nominal time increased, both $LMA_P{}^a$ and $LMA_P{}^b$ increased linearly. The slope of $LMA_P{}^a$ is greater than that of $LMA_P{}^b$. The combined LMA by total supply air, $LMA_P{}^c$, falls between the two sets. The figure also shows the LMA data calculated from the individual LMAs using Eq. (12).

The LMA values at the exhaust are expressed with respect to the nominal time constant in Fig. 20(b). The individual LMAs at exhaust indicate the residence time of the air supplied

through the corresponding inlets. The longer the individual LMA, the longer the corresponding supply air resides in the space. The combined LMAs are in the midst of individual LMAs, all of which vary linearly with respect to the nominal time constant. The weighted averages calculated from the individual LMAs are also shown in the figure. Notice that the weighting factors at exhaust are both 0.5 in this case, since the airflow rates are the same for both inlets. Theoretically, the combined LMA should be the same with the nominal time constant regardless of the airflow rates, which is shown by a solid line in the figure. We note that the combined LMAs appeared within the 10% error band.



(a) LMA at P. (b) LMA at exhaust.

Fig. 20. Local mean ages of supply air at point P and at the exhaust as a function of nominal time constant.

6.3.5 Concluding remarks

In this example, a case of multiple inlets was considered. The relations between LMA values from individual inlets and the combined LMA were obtained experimentally in a simplified model space simulating livestock applications. The following conclusions are drawn from these results.

1. Our experimental results confirmed the theoretical relation between the individual LMAs and the combined LMA of the total supply air. The weighting factors are the steady concentrations obtained with a continuous step-up tracer injection at the corresponding supply inlets.
2. At every point in the space, the non-dimensional steady concentrations are complimentary to each other. The non-dimensional steady concentration at a point can be considered as a relative contribution factor of an individual inlet to the supply characteristics at the point.
3. The spatial distribution of an individual LMA indicates how fast the supply air from the corresponding inlet can reach the space, and it is closely related to the airflow pattern in the space.
4. These experimental procedures were verified by the fact that the overall local mean ages at the exhaust are in good agreement with the nominal time constants.

The concepts and the relations developed in this study can be applied to various applications to quantify supply characteristics of individual inlets.

7. Conclusion

The purpose of ventilation is to supply fresh air to an occupied space and to effectively remove contaminants generated within the space. Ventilation performance is determined not only by the air change rate, but also by the ventilation effectiveness.

This study dealt with ventilation effectiveness based on the concept of the age of air. Ventilation effectiveness was categorized into supply effectiveness and exhaust effectiveness. The local supply index was represented by the local mean age of supply air; similarly, the local exhaust index was represented by local mean residual-life-time of contaminant. Overall room ventilation effectiveness was expressed as one value, regardless of supply and exhaust, because the room average of the local supply index was found to be identical to that of the local exhaust index.

The age concept has been extended to a space with multiple inlet and outlet openings. Theoretical derivations were made to obtain the relations between the LMAs from individual inlets and the combined LMA of total supply air, as well as the relations between the LMRs toward individual outlets and the overall LMR of the total exhaust air. Those relations can be used to investigate the effect of each supply inlet among many inlets, and the contribution of each exhaust outlet among many outlets in a space with multiple inlets and outlets.

The tracer gas technique provided a powerful tool in our ventilation studies for measuring the ventilation effectiveness of a conditioned space as well as to evaluate the performance of diffusers and exhaust grills. The ventilation theories provided in this chapter can be applied to various applications to provide good indoor air quality and to save ventilation energy use in buildings.

8. Appendix

It can be easily proved that the local mean age distribution in a space is equivalent to the steady concentration distribution with uniformly distributed sources of unit strength in the space.

The general equation that governs the transient concentration distribution can be expressed as

$$\frac{\partial C}{\partial t} + \vec{v} \cdot \nabla C = \nabla \cdot (D \nabla C) + \dot{m} \tag{A1}$$

where D is the diffusion coefficient of the contaminant in air. Consider the case of a step-down procedure with no contaminant source in the space. By integrating Eq. (A1) from zero to infinity with $\dot{m}$ equal to zero, we obtain

$$C(\infty) - C(0) + \vec{v} \cdot \nabla \int_0^\infty C dt = \nabla \cdot (D \nabla \int_0^\infty C dt) \tag{A2}$$

The steady concentration is zero; thus, Eq. (A2) can be rewritten as

$$\vec{v} \cdot \nabla \left[\int_0^\infty \frac{C}{C(0)} dt \right] = \nabla \cdot (D \nabla \left[\int_0^\infty \frac{C}{C(0)} dt \right]) + 1 \tag{A3}$$

The expression in the bracket is the local mean age under a step-down procedure.

On the other hand, Eq. (A1) can be simplified for steady concentration with uniformly distributed sources. As $\dot{m}$ is constant through the space, the equation can be simplified as

$$\vec{v} \cdot \nabla \frac{C}{\dot{m}} = \nabla \cdot (D \nabla \frac{C}{\dot{m}}) + 1 \tag{A4}$$

Therefore, the steady concentration divided by the source strength equals the local mean age in the space:

$$\therefore \int_0^\infty \frac{C}{C(0)} dt = \frac{\bar{C}(\infty)}{\dot{m}} \tag{A5}$$

9. References

AIVC, (1990). A Guide to Air Change Efficiency, Technical Note AIVC28, Air Infiltration and Ventilation Centre, Coventry, United Kingdom.

ASHRAE, (2009). *ASHRAE Handbook-Fundamentals*, American Society of Heating, Refrigerating, and Air-Conditioning Engineers, Atlanta, USA.

ASTM, (1993). Standard Test Methods for Determining Air Change in a Single Zone by Means of a Tracer Gas Dilution, E741-93, American Society for Testing and Materials, USA.

Corpron, M. H. (1992). *Design and Characterization of a Ventilation Chamber*, M.S. Thesis. Department of Mechanical Engineering, University of Minnesota, Minneapolis, USA.

Danckwerts, P. V. (1958). Local Residence-Times in Continuous-Flow Systems, *Chemical Engineering Science*, Vol. 9, pp. 78-79.

Dufton, A. F. & Marley, W. G. (1935). Measurement of Rate of Air Change, Institution of Heating and Ventilating Engineers, Vol. 1, p. 645.

Etheridge, D. & Sandberg, M. (1996). *Building Ventilation: Theory and Measurement*, John Wiley & Sons, New York, USA.

Han, H. (1992). Calculation of Ventilation Effectiveness Using Steady-State Concentration Distributions and Turbulent Airflow Patterns in a Half Scale Office Building, Proc. of Int.l Symp. on Room Air Convection and Ventilation Effectiveness, pp. 187-191, Tokyo, Japan.

Han, H.; Kuehn, T. H. & Kim, Y. I. (1999). Local Mean Age Measurements for Heating, Cooling, and Isothermal Supply Air Conditions, *ASHRAE Trans*., Vol. 105, Pt. 2, pp. 275-282.

Han, H.; Choi, S. H. & Lee, W. W. (2002). Distribution of Local Supply and Exhaust Effectiveness according to Room Airflow Patterns, *International Journal of Air-conditioning and Refrigeration,* Vol. 10, No. 4, pp. 177-183.

Han, H.; Shin, C. Y.; Lee, I.B. & Kwon, K. S. (2010). Local Mean Ages of Air in a Room with Multiple Inlets, *Int. J. of Air-Conditioning and Refrigeration*, Vol. 18, No. 1, pp. 15-21.

Han, H.; Shin, C. Y.; Lee, I.B. & Kwon, K. S. (2011). Tracer Gas Experiment for Local Mean Ages of Air from Individual Supply Inlets in a Space with Multiple Inlets, *Building and Environment*, Vol. 46, pp. 2462-2471.

Kuehn, T. H.; Ramsey, J. W. & Threlkeld, J. L. (1998). *Thermal Environmental Engineering*, 3rd ed., Prentice Hall, London, United Kingdom.

Liang, H. (1994). Room Air Movement and Contaminant Transport, *Ph.D. Thesis*. Department of Mechanical Engineering, University of Minnesota, Minneapolis, USA.

Sandberg, M. (1981). What is Ventilation Efficiency, *Building and Environment*, Vol. 16, No. 2, pp. 123-135.

Sandberg, M. & Sjoberg, M. (1983). The Use of Moments for Assessing Air Quality in Ventilated Rooms, *Building and Environment*, Vol. 18, No. 4, pp. 181-197.

Shaw, C. Y., Zhang, J. S., Said, M. N. A., Vaculik, F. & Magee, R. J. (1992). Effect of Air Diffuser Layout on the Ventilation Conditions of a Workstation-Part II: Air Change Efficiency and Ventilation Efficiency, *ASHRAE Trans.,* Vol. 99, Pt. 2, pp. 133-143.

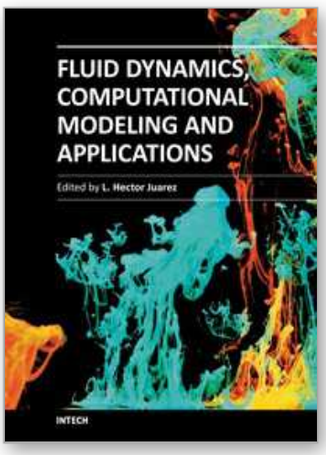
Skaaret, E. (1986). Contaminant Removal Performance in Terms of Ventilation Effectiveness, *Environmental International*, Vol. 12, Issues 1-4, pp. 419-427.

Spalding, D. B. (1958). A Note on Mean Residence-Times in Steady Flows of Arbitrary Complexity, *Chemical Engineering Science*, Vol. 9, pp. 74-77.

Yaglou, C. P. & Witheridge W. N. (1937). Ventilation Requirements, *ASHVE Trans*., Vol. 42, pp. 423-436.

Xing, H., Hatton, A. & Awbi, H. B. (2001). A Study of the Air Quality in the Breathing Zone in a Room with Displacement Ventilation, *Building and Environment*, Vol. 36, pp. 809-820.

IntechOpen



Fluid Dynamics, Computational Modeling and Applications

Edited by Dr. L. Hector Juarez

ISBN 978-953-51-0052-2
Hard cover, 660 pages
Publisher InTech
Published online 24, February, 2012
Published in print edition February, 2012

The content of this book covers several up-to-date topics in fluid dynamics, computational modeling and its applications, and it is intended to serve as a general reference for scientists, engineers, and graduate students. The book is comprised of 30 chapters divided into 5 parts, which include: winds, building and risk prevention; multiphase flow, structures and gases; heat transfer, combustion and energy; medical and biomechanical applications; and other important themes. This book also provides a comprehensive overview of computational fluid dynamics and applications, without excluding experimental and theoretical aspects.

How to reference

In order to correctly reference this scholarly work, feel free to copy and paste the following:

Hwataik Han (2012). Ventilation Effectiveness Measurements Using Tracer Gas Technique, Fluid Dynamics, Computational Modeling and Applications, Dr. L. Hector Juarez (Ed.), ISBN: 978-953-51-0052-2, InTech, Available from: http://www.intechopen.com/books/fluid-dynamics-computational-modeling-and-applications/ventilation-effectiveness-measurements-using-tracer-gas-technique

INTECH
open science | open minds

InTech Europe
University Campus STeP Ri
Slavka Krautzeka 83/A
51000 Rijeka, Croatia
Phone: +385 (51) 770 447
Fax: +385 (51) 686 166
www.intechopen.com

InTech China
Unit 405, Office Block, Hotel Equatorial Shanghai
No.65, Yan An Road (West), Shanghai, 200040, China
中国上海市延安西路65号上海国际贵都大饭店办公楼405单元
Phone: +86-21-62489820
Fax: +86-21-62489821

© 2012 The Author(s). Licensee IntechOpen. This is an open access article distributed under the terms of the Creative Commons Attribution 3.0 License, which permits unrestricted use, distribution, and reproduction in any medium, provided the original work is properly cited.

IntechOpen

IntechOpen